

Machine learning of complex conductivity anisotropy

Charles L. Bérubé & Jean-Luc Gagnon

Polytechnique Montréal

Introduction

Considering the Earth's crust's omnipresent anisotropy, accurate simulations of geoelectric data must account for induced polarization (IP) effects in three dimensions.

The Generalized Effective Medium Theory of Induced Polarization (GEMTIP, Zhdanov, 2008) models IP effects in three dimensions at the rock scale (Alfouzan et al., 2020), rather than mechanically at the grain scale (Revil and Cosenza, 2010). However, GEMTIP simulations that consider realistic rock models derived from mineralogical analyses (e.g., Bérubé et al., 2018; Gurin et al., 2018; Zhdanov et al., 2018) require solving the depolarization tensors of each mineral inclusion numerically and may be subject to prohibitive computation times.

This research aims to streamline GEMTIP simulations for realistic rock models by simultaneously solving all depolarization tensor elements with a neural network.

Key variables

(x, y, z) and (θ, ϕ) are coordinates.
 a, b, c are the semi-axes lengths of the ellipsoids.
 $\sigma_b = \text{diag}(\sigma_{b,x}, \sigma_{b,y}, \sigma_{b,z})$ is background conductivity.
 $A, B = b/a, c/a$ are ellipsoid shape ratios.
 $C, D = \sigma_{b,y}/\sigma_{b,x}, \sigma_{b,z}/\sigma_{b,x}$ are conductivity ratios.

Anisotropic depolarization tensors

The accumulation of charges on the surface of mineral grains results in a voltage perturbation ΔU , which is assumed proportional to the normal current, such that

$$\Delta U = \kappa(\hat{\mathbf{n}} \cdot \mathbf{J}), \quad (1)$$

where $\hat{\mathbf{n}}$ is a unit vector normal to the grain surface, \mathbf{J} is the current density and $\kappa = \lambda(i\omega)^{-\rho}$ is a function of the imaginary unit i , angular frequency ω , surface polarizability λ and relaxation parameter ρ (Zhdanov, 2008).

Bérubé and Gagnon (2024) derive the anisotropic depolarization tensors. The volume depolarization tensor is

$$\mathbf{\Gamma} = -\frac{abc}{4\pi\sigma_s} \mathbf{T} \int_0^{2\pi} \int_0^\pi \frac{d\theta d\phi |\sin\theta|}{|\mathbf{R}'|^3} \mathbf{n}' \mathbf{R}', \quad (2)$$

and the surface depolarization tensor is

$$\mathbf{\Lambda} = -\frac{abc}{4\pi\sigma_s} \int_0^{2\pi} \int_0^\pi \frac{d\theta d\phi \sin\theta}{|\mathbf{R}'|^5 |\mathbf{n}'|} \mathbf{Q}', \quad (3)$$

where

$$\mathbf{r}' = a \sin(\theta) \cos(\phi) \hat{\mathbf{x}} + b \sin(\theta) \sin(\phi) \hat{\mathbf{y}} + c \cos(\theta) \hat{\mathbf{z}},$$

$$\mathbf{n}' = a^{-1} \sin(\theta) \cos(\phi) \hat{\mathbf{x}} + b^{-1} \sin(\theta) \sin(\phi) \hat{\mathbf{y}} + c^{-1} \cos(\theta) \hat{\mathbf{z}},$$

$$\mathbf{Q}' = (-3(\mathbf{R}'\mathbf{R}') + |\mathbf{R}'|^2 \mathbf{I}) \mathbf{n}' \mathbf{n}'^T, \quad \mathbf{T} = \sigma_b^{-1/2}, \quad \mathbf{R}' = \mathbf{T} \mathbf{r}',$$

and $\sigma_s = \det(\sigma_b)^{1/2}$.

Equations 2 and 3 must be solved numerically with Simpson's Rule integration (SRI), for example.

Effective medium conductivity

Zhdanov (2008) defines the conductivity tensor σ as the sum of the background conductivity σ_b and a conductivity perturbation $\Delta\sigma$. The effective conductivity of a rock containing N polarizable inclusions is

$$\sigma_{\text{eff}} = \sigma_b + \sum_{i=1}^N [\mathbf{I} + \mathbf{p}_i]^{-1} [\mathbf{I} - (\mathbf{I} + \mathbf{p}_i) \Delta\sigma_i \mathbf{\Gamma}_i]^{-1} [\mathbf{I} + \mathbf{p}_i] \Delta\sigma_i \nu_i, \quad (4)$$

where \mathbf{I} is the identity matrix and ν_i is the volumetric fraction of the i^{th} inclusion. Additionally, $\mathbf{p}_i = \xi_i \mathbf{\Gamma}_i^{-1} \mathbf{\Lambda}_i$ is the surface polarizability and $\xi_i \approx \kappa(\Delta\sigma)^{-1} \sigma_b \sigma$.

Rotation of the inclusions

To simulate a realistic effective rock medium, we define mineral inclusions of any orientation with

$$\mathbf{\Gamma}_{\text{rot}}, \mathbf{\Lambda}_{\text{rot}} = \mathbf{S} \mathbf{\Gamma} \mathbf{S}^T, \mathbf{S} \mathbf{\Lambda} \mathbf{S}^T, \quad (5)$$

where $\mathbf{\Gamma}_{\text{rot}}$ and $\mathbf{\Lambda}_{\text{rot}}$ are rotated depolarization tensors and \mathbf{S} is a rotation matrix defined by Euler angles α about the x axis, β about the y axis and γ about the z axis.

Neural network approximation

We use a multilayer perceptron (MLP) with $K = 4$ hidden layers. The MLP output aims to approximate the volume and surface depolarization tensors and is defined as

$$\hat{\mathbf{\Lambda}} \hat{\mathbf{\Gamma}} = (\mathbf{W}^{(K+1)} \mathbf{a}^{(K)} + \mathbf{b}^{(K+1)}), \quad (6)$$

where the output of the k^{th} hidden layer is

$$\mathbf{a}^{(k)} = \text{SiLU}(\mathbf{W}^{(k)} \mathbf{a}^{(k-1)} + \mathbf{b}^{(k)}). \quad (7)$$

$\mathbf{W}^{(k)}$ and $\mathbf{b}^{(k)}$ are the MLP weights and biases. The input is $\mathbf{a}^{(0)} = (A, B, C, D)$. SiLU is a sigmoid linear unit activation function. Figure 1 shows the MLP training strategy.

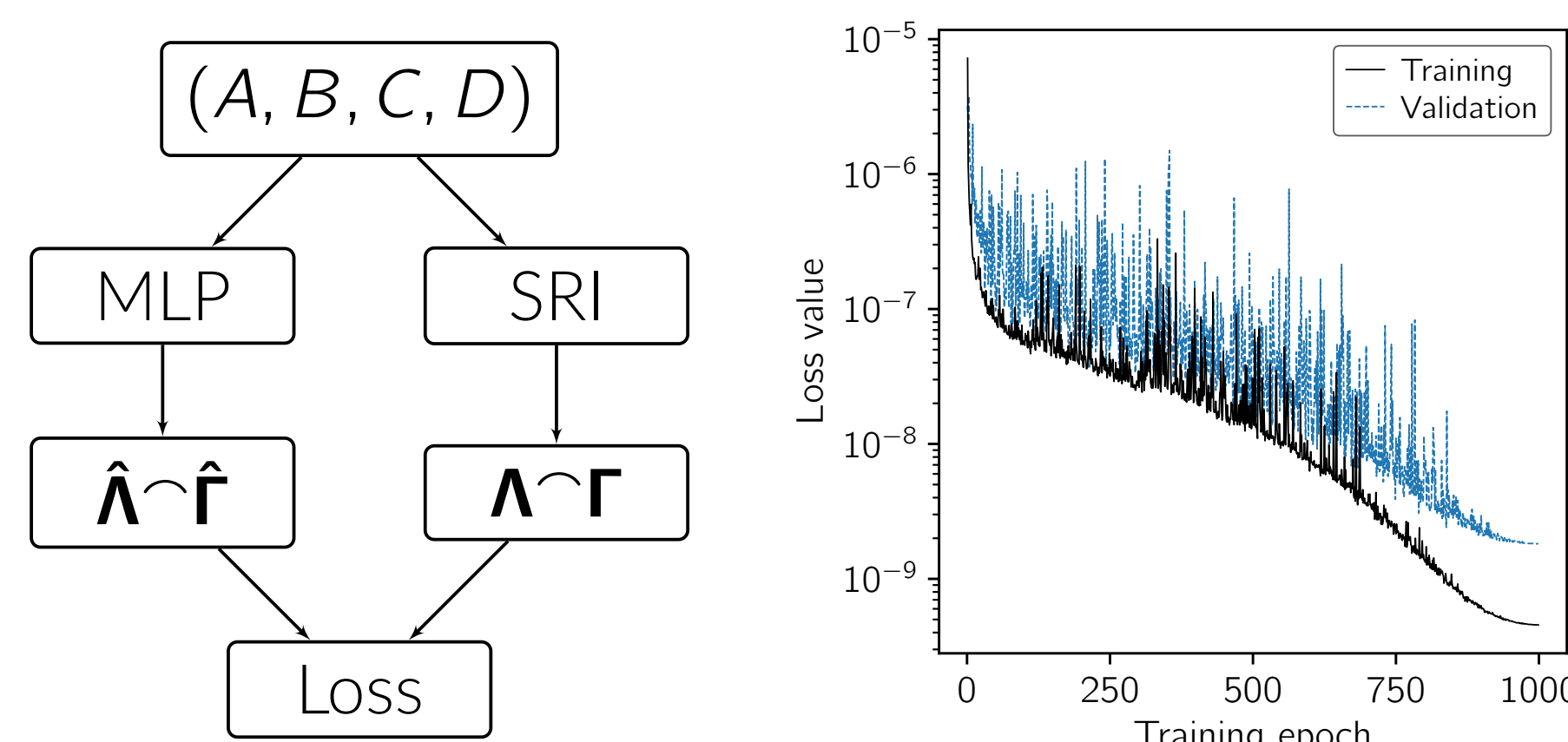
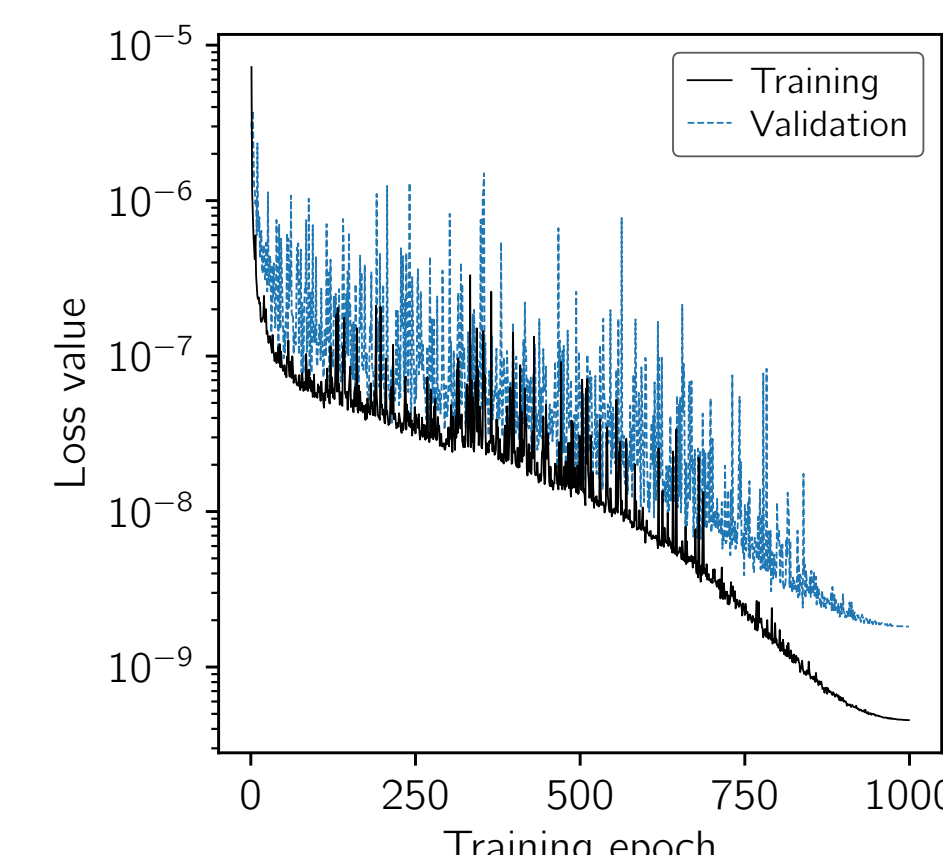


Figure 1. MLP training flowchart. Figure 2. MLP learning curves.



We optimize $\mathbf{W}^{(k)}$ and $\mathbf{b}^{(k)}$ using the backward propagation algorithm and Adam optimizer (Kingma and Ba, 2015), a batch size of 32 and a one-cycle maximum learning rate of 10^{-2} . The loss function we use is

$$\text{Loss} = \|\hat{\mathbf{\Lambda}} \hat{\mathbf{\Gamma}} - \mathbf{\Lambda} \mathbf{\Gamma}\|_2^2. \quad (8)$$

Figure 2 shows the loss as a function of training epochs.

Validation metrics

We evaluate the number of exact significant digits with

$$p = -\log_{10} \left| \frac{\hat{\mathbf{\Gamma}}, \hat{\mathbf{\Lambda}} - \mathbf{\Gamma}, \mathbf{\Lambda}}{\mathbf{\Gamma}, \mathbf{\Lambda}} \right|, \quad (9)$$

and the prediction bias with

$$r = \log_{10} \left(\frac{\hat{\mathbf{\Gamma}}, \hat{\mathbf{\Lambda}}}{\mathbf{\Gamma}, \mathbf{\Lambda}} \right), \quad (10)$$

which should be symmetric with respect to the origin.

Neural network analysis

The volume depolarization tensor is more sensitive to host rock conductivity, whereas the surface depolarization tensor is more sensitive to inclusion shape (Table 1).

Table 1. Relative sensitivity indices of the MLP (in %).

	Shape (A, B)	Conductivity (C, D)
Volume ($\mathbf{\Gamma}$)	47.80 ± 0.06	52.20 ± 0.08
Surface ($\mathbf{\Lambda}$)	64.53 ± 0.05	35.47 ± 0.07

For weakly anisotropic materials ($ABCD > 0.1$ in Figure 3), the MLP predicts up to four exact significant digits with a negligible bias. For highly anisotropic materials ($ABCD \ll 0.1$), the MLP precision decreases to two exact significant digits while its prediction bias increases.

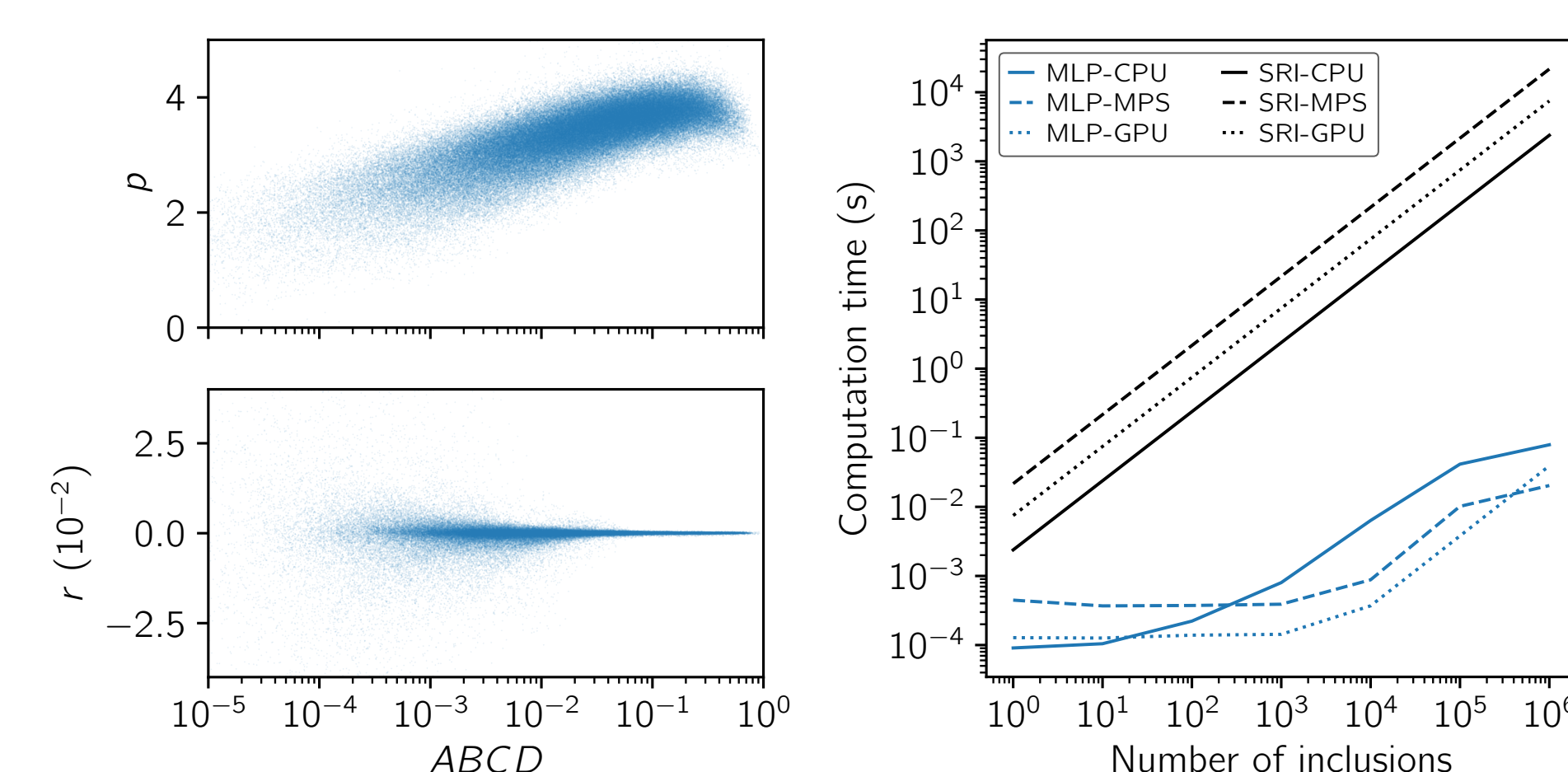
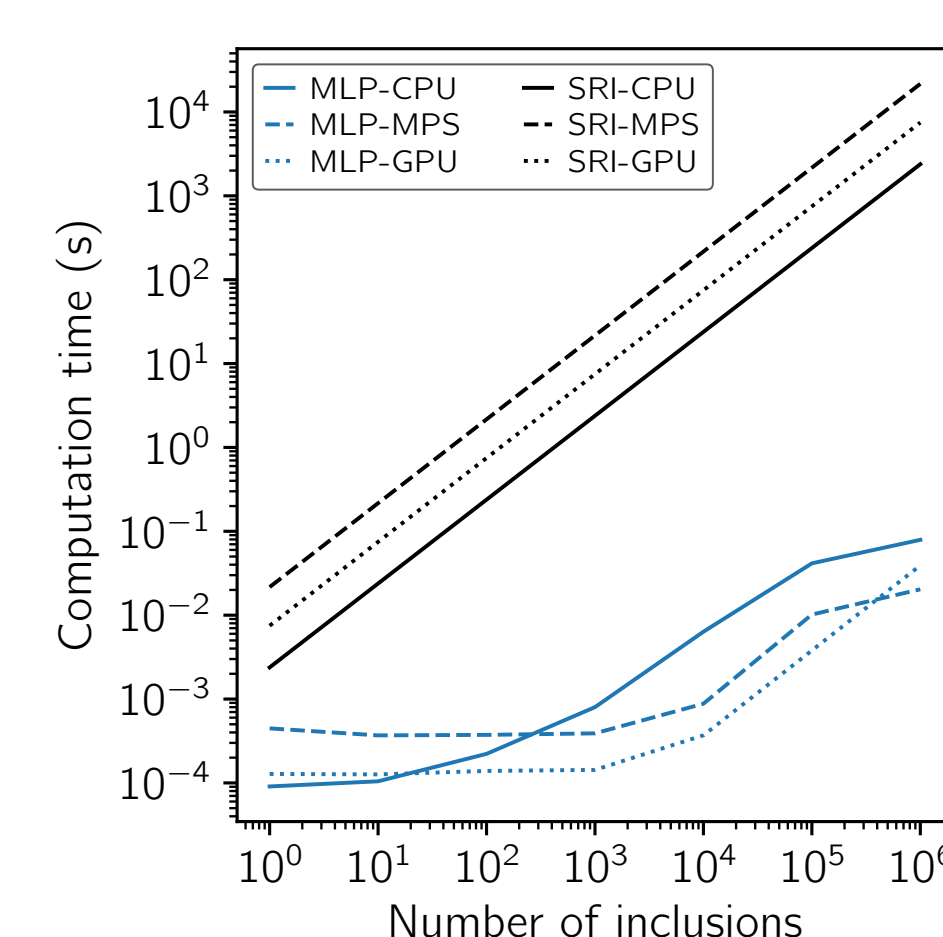


Figure 3. Validation metrics. Figure 4. Computation times.



Remarkably, SRI takes up to 10^4 seconds to solve the depolarization tensors of one million inclusions, whereas the MLP performs this task in only 10^{-1} second (Figure 4).

Application to real rock samples

We test the MLP using an actual metasedimentary rock sample (K389055) from the sulfide-associated Canadian Malartic disseminated gold deposit. Extensive quantitative mineralogy analyses and complex resistivity measurements of sample K389055 are described in Bérubé et al. (2018). Figure 5 shows one of 1708 backscatter electron images from petrographic thin sections of sample K389055, and Figure 6 shows the grain statistics of this sample derived from mineral liberation analysis.

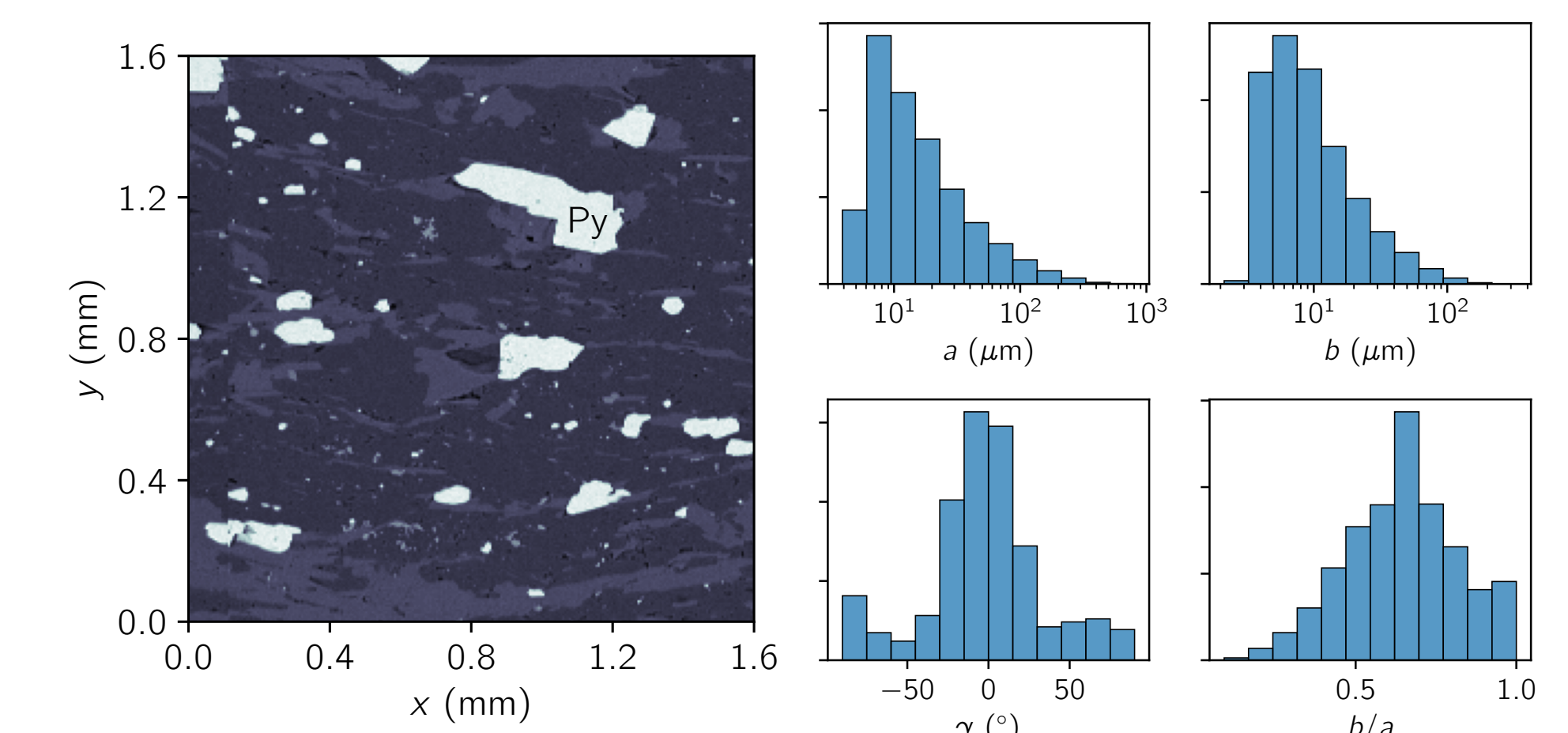


Figure 5. Backscatter electron image of sample K389055. Figure 6. Pyrite grain statistics of sample K389055.

In Figure 7, we illustrate an effective medium based on the grain statistics of sample K389055, assuming that mineral grains are triaxial ellipsoids (c values are randomly drawn from the a and b grain size distributions).

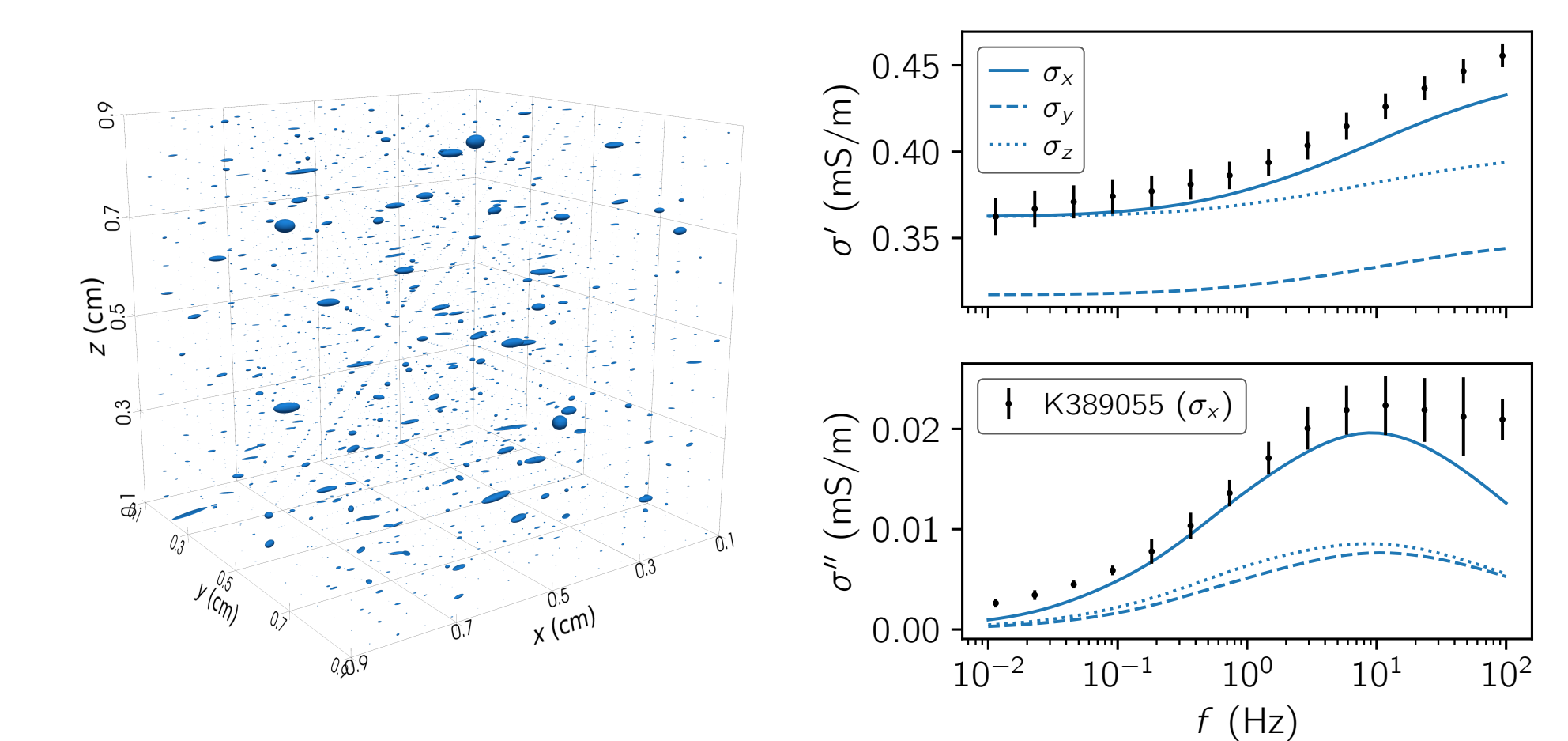


Figure 7. Effective medium derived from sample K389055. Figure 8. Effective complex conductivity of sample K389055.

Finally, Figure 8 shows the measured and modelled complex conductivity of sample K389055. We use the field-measured background conductivity anisotropy values of Mir et al. (2018) for Canadian Malartic in the simulation.

Conclusions

Neural networks can streamline IP modelling for anisotropic rocks by simultaneously solving the depolarization tensors of numerous mineral inclusions. After extensive model validation, we test the MLP by simulating the effective complex conductivity of real rock samples. Based on effective medium theory, the model predictions are compatible with previously published IP measurements performed in one direction. Results show that machine learning is a fast and precise alternative to numerical integration for solving depolarization tensors, making it practical to simulate the IP responses of realistic rock models with limited computational resources.

References

- Alfouzan, F. A., Alotaibi, A. M., Cox, L. H., and Zhdanov, M. S. (2020). Spectral Induced Polarization Survey with Distributed Array System for Mineral Exploration. *Minerals*, 10:769.
- Bérubé, C. L. and Gagnon, J.-L. (2024). Anisotropic induced polarization modeling with neural networks and effective medium theory. arXiv:2402.11313 [physics].
- Bérubé, C. L., Olivo, G. R., Chouteau, M., and Perrouty, S. (2018). Mineralogical and textural controls on spectral induced polarization signatures of the Canadian Malartic gold deposit: Applications to mineral exploration. *Geophysics*, 84:B135–B151.
- Gurin, G., Ilyin, Y., Nilov, S., Ivanov, D., Kozlov, E., and Titov, K. (2018). Induced polarization of rocks containing pyrite: Interpretation based on X-ray computed tomography. *Journal of Applied Geophysics*, 154:50–63.
- Kingma, D. P. and Ba, J. (2015). Adam: A Method for Stochastic Optimization. In Bengio, Y. and LeCun, Y., editors, *3rd International Conference on Learning Representations, ICLR 2015, San Diego, CA, USA, May 7–9, 2015, Conference Track Proceedings*, pages 8024–8035.
- Mir, R., Perrouty, S., Astic, T., Bérubé, C. L., and Smith, R. S. (2018). Structural complexity inferred from anisotropic resistivity: Example from airborne EM and compilation of historical resistivity/induced polarization data from the gold-rich Canadian Malartic district. *Geophysics*, 84(2):B153–B167.
- Revil, A. and Cosenza, P. (2010). Comment on "Generalized effective-medium theory of induced polarization". *Geophysics*, 75:X7–X9.
- Zhdanov, M. (2008). Generalized effective-medium theory of induced polarization. *Geophysics*, 73:F197–F211.
- Zhdanov, M. S., Burtman, V., Endo, M., and Lin, W. (2018). Complex resistivity of mineral rocks in the context of the generalised effective-medium theory of the induced polarisation effect. *Geophysical Prospecting*, 66:798–817.